Computational Aeroacoustics: An Overview

Christopher K.W. Tam
Department of Mathematics, Florida State University
Tallahassee, FL 32306-4510, USA

Abstract

An overview of recent advances in computational aeroacoustics (CAA) is presented. CAA algorithms must not be dispersive and dissipative. It should propagate waves supported by the Euler equations with the correct group velocities. Computation domains are inevitably finite in size. To avoid the reflection of acoustic and other outgoing waves at the boundaries of the computation domain, it is required that special boundary conditions be imposed at the boundary region. These boundary conditions either absorb all the outgoing waves without reflection or allow the waves to exit smoothly. High-order schemes, invariably, supports spurious short waves. These spurious waves tend to pollute the numerical solution. They must be selectively damped or filtered out. All these issues and relevant computation methods are briefly reviewed. Jet screech tones are known to have caused structural fatigue in military combat aircrafts. Numerical simulation of the jet screech phenomenon is presented as an example of a successful application of CAA.

1. Introduction

Aeroacoustic problems are by nature very different from standard aerodynamics and fluid mechanics problems. Before discussing how to solve aeroacoustics problems numerically or simulate them computationally, an approach generally referred to as Computational Aeroacoustics (CAA), it is important to recognize and to have a good understanding of these differences. These differences pose a number of major challenges to CAA. A few of the important computational challenges are listed below.

a. Aeroacoustics problems, by definition, are time dependent, whereas aerodynamics and fluid mechanics problems are generally time independent or involve only low frequency unsteadiness.

b. Aeroacoustics problems typically involve frequency range that spreads over a wide bandwidth. Numerical resolution of the high frequency waves becomes a formidable obstacle to accurate numerical simulation.

c. Acoustic waves usually have small amplitudes. They are very small compared to the mean flow. Oftentimes, the sound intensity is five to six orders smaller. To compute sound waves accurately, a numerical scheme must have extremely low numerical noise.

d. In most aeroacoustics problems, interest is in the sound waves radiating to the far field. This requires a solution that is uniformly valid from the source region all the way to the measurement point at many acoustic wavelengths away. Because of the long propagation distance, computational aeroacoustics schemes must have minimal numerical dispersion and dissipation. Also, it should propagate the waves at the correct wave speeds and is isotropic irrespective of the orientation of the computation mesh.

e. In general, flow disturbances in aerodynamics or fluid mechanics problems tend to decay exponentially fast away from a body or their source of generation. Acoustic waves, on the other hand, decay very slowly and actually reach the boundaries of a finite computation domain. To avoid the reflection of outgoing sound waves back into the computation domain, radiation boundary conditions must be imposed at the artificial exterior boundaries to assist the waves to exit smoothly. For standard computation fluid dynamics (CFD) problems, such boundary conditions are usually not required.

Paper presented at the RTO AVT Symposium on "Ageing Mechanisms and Control: Part A – Developments in Computational Aero- and Hydro-Acoustics", held in Manchester, UK, 8-11 October 2001, and published in RTO-MP-079(I).

f. Aeroacoustics problems are archtypical examples of multiple-scales problems. The length scale of the acoustic source is usually very different from the acoustic wave length. That is, the length scale of the source region and that of the acoustic far field region can be vastly different. Computational aeroacoustic methods must be designed to deal with problems with greatly different length scales in different parts of the computational domain,

It must be acknowledged that CFD has been very successful in solving fluid and aerodynamics problems. CFD methods are generally designed for computing time independent solutions. Because of the tremendous success of CFD, it is tempting to use these methods to solve aeroacoustics problems as well. In the past, there have been a number of attempts to do just that. However, the results have proven to be quite discouraging. For example, Hsi and Perie tried to use a commercial CFD code "RADIOSS" to solve sound scattering problems. Their effort was published in the proceedings of the Second CAA Workshop on Benchmark Problems (NASA CP3352, June 1997, edited by C.K.W. Tam and J.C. Hardin). The results were disastrous. The computed results were highly dispersive and differed significantly from the exact solutions.

As elaborated above, it should be clear that the nature of aeroacoustics problems are substantially different from those of traditional fluid dynamics and aerodynamics problems. To be able to compute or simulate aeroacoustics problems accurately and efficiently, standard CFD schemes, designed for applications to fluid problems, are generally not adequate. For this reason, there is a need for an independent development of CAA. This was what happened in the last ten years. During this period, great advances have been made both in the development of CAA methodology and in their applications to real world problems.

To simulate an aeroacoustic phenomenon or problem numerically, the computation algorithm must consist of three basic elements. They are:

(i) A time marching computation scheme.

(ii) An artificial selective damping algorithm or filtering procedure.

(iii) A set of radiation/outflow numerical treatments for use at the boundaries of the computation domain.

A good quality time marching scheme is basic to any computation effort. Artificial selective damping or a filtering procedure is essential to eliminating spurious numerical waves that could contaminate the computed solution. Also such damping terms can often help to suppress numerical instabilities at the boundaries of the computation domain or at surfaces of discontinuities such as mesh-size-change interfaces. Numerical boundary treatments serve two basic purposes. First, they are to allow outgoing waves to leave the computation domain with little reflection. Second, they are to reproduce all the effects of the outside world on the computation domain. For instance, if there is incoming acoustic and vorticity wave or there is an inflow, they are to be generated by the numerical boundary conditions.

2. Spatial Discretization in Wavenumber Space

In this section, we consider how to form finite difference approximations to the partial derivatives of spatial coordinates. The standard approach of truncated Taylor series assumes that the mesh size goes to zero; i.e., $\Delta x \to 0$, in formulating finite difference approximation. In real applications, Δx is never equal to zero. Therefore, we will investigate how well we can approximate $\partial/\partial x$ by a finite difference quotient with a finite Δx. The treatment below follows the work of Tam and Webb[1] and Tam[2]

Suppose we use a $(2N+1)$ point stencil to approximate $\partial/\partial x$; i.e.,

$$\left(\frac{\partial f}{\partial x}\right)_t \cong \frac{1}{\Delta x}\sum_{j=-N}^{N} a_j f_{t+j}. \tag{2.1}$$

At our disposal are the coefficients a_j; j=$-N$ to N. We will now choose these coefficients such that the Fourier Transform of the right side of (2.1) is a good approximation of that of the left side, for arbitrary function f. Fourier Transform is defined only for functions of a continuous variable. Let's first generalize

(2.1) to all points along the x-axis. The generalized form of (2.1), applicable to any set of points at Δx apart, is

$$\left(\frac{\partial f}{\partial x}\right)(x) \cong \frac{1}{\Delta x}\sum_{-N}^{N} a_j f(x + j\Delta x). \tag{2.2}$$

(2.1) is a special case of (2.2). By setting $x = \ell\,\Delta x$ in (2.2), (2.1) is recovered.

The Fourier Transform of a function $F(x)$ and its inverse are related by

$$\tilde{F}(\alpha) = \frac{1}{2\pi}\int_{-\infty}^{\infty} F(x)e^{-i\alpha x}dx, \quad F(x) = \int_{-\infty}^{\infty}\tilde{F}(\alpha)e^{i\alpha x}d\alpha. \tag{2.3}$$

Now by applying Fourier Transform to (2.2) and making use of the Derivative and Shifting Theorems, it is found

$$i\alpha\tilde{f} \cong \frac{1}{\Delta x}\left[\sum_{j=-N}^{N} a_j e^{ij\alpha\Delta x}\right]\tilde{f} = i\bar{\alpha}\tilde{f} \tag{2.4}$$

where

$$\bar{\alpha} = \frac{-i}{\Delta x}\sum_{j=-N}^{N} a_j e^{ij\alpha\Delta x}. \tag{2.5}$$

Clearly, $\bar{\alpha}$ is the effective wave number of the finite difference scheme. $\bar{\alpha}\,\Delta x$ is a periodic function of $\alpha\Delta x$ with a period of 2π. To assure that the Fourier transform of the finite difference scheme is a good approximation of that of the partial derivative over the band of wavenumber $\eta \le \alpha\Delta x \le \eta$, it is required that a_j be chosen to minimize the integrated error, E, over this wavenumber range, where,

$$E = \int_{-\eta}^{\eta} \left|\alpha\Delta x - \bar{\alpha}\Delta x\right|^2 d(\alpha\Delta x). \tag{2.6}$$

For $\bar{\alpha}$ to be real, the coefficients a_j must be antisymmetric; i.e.,

$$a_0 = 0, \qquad a_{-j} = -a_j \tag{2.7}$$

The conditions for E to be a minimum are,

$$\frac{\partial E}{\partial a_j} = 0, \qquad j = 1,2,\ldots,N. \tag{2.8}$$

(2.8) provides N equations for the N coefficients a_j, j=1,2,...,N.

For a 7-point stencil (N=3) there are three coefficients. It is possible to require (2.2) to be accurate to $O(\Delta x^4)$ by Taylor series expansion. This leaves one free parameter for optimization. By setting η=1.1, it is easy to find,

$$a_0 = 0.0, \qquad a_1 = -a_{-1} = 0.77088238051822552,$$

$$a_2 = -a_{-2} = -0.166705904414580469, \quad a_3 = -a_{-3} = 0.02084314277031176.$$

The choice of η=1.1 turns out to provide an overall best group velocity approximation[2].

The relationship between $\bar{\alpha}\,\Delta x$ and $\alpha\Delta x$ over the interval 0 to π for the optimized 7-point stencil is shown graphically in Figure 1. For $\alpha\Delta x$ up to about 1.2, the curve is nearly the same as the straight line $\bar{\alpha}\,\Delta x = \alpha\Delta x$. Thus, the finite difference scheme can provide reasonable approximation to $\alpha\Delta x < 1.2$ or $\lambda > 5.2\Delta x$ where λ is the wavelength. For $\alpha\Delta x$ greater than 2, the $\bar{\alpha}(\alpha)$ curve deviates increasingly from the straight-line relationship. Thus, the wave propagation characteristics of the short waves of the finite difference scheme are very different from those of the partial differential equations. Figure 1 also shows the $\bar{\alpha}\,\Delta x$ versus $\alpha\Delta x$ relations for the standard 6th-order, 4th-order and 2nd-order central difference schemes. Their resolved bandwidth is narrower. In other words, more mesh points per wavelength is needed for propagating a wave accurately.

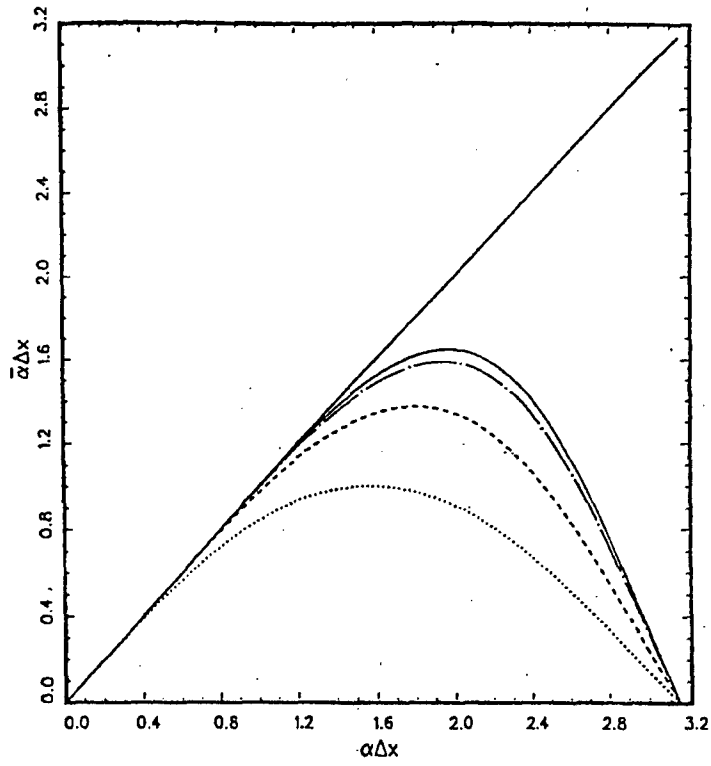

Figure 1. $\bar{\alpha}\Delta x$ versus $\alpha\Delta x$. ———— optimized 4th-order scheme, — · — · — · standard 6th-order scheme, - - - - - - - standard 4th-order scheme, ····· standard 2nd-order scheme.

Example. Let us consider the initial value problem of the one-dimensional convective wave equation. We will use dimensionless variables with Δx as the length scale, $\Delta x/c$ (c= sound speed) as the time scale. The mathematical problem is:

$$\frac{\partial u}{\partial t}+\frac{\partial u}{\partial x}=0, \qquad -\infty < x < \infty \tag{2.9}$$

$$t=0, \qquad u=f(x) \tag{2.10}$$

The exact solution is

$$u=f(x-t).$$

In other words, the solution consists of the initial disturbance propagating to the right at a dimensionless speed of 1, without any distortion of the waveform. Let us consider the initial disturbance in the form of a Gaussian function,

$$f(x)=0.5\ \exp\left[-\ell n2\left(\frac{x}{3}\right)^2\right]. \tag{2.11}$$

On using a $(2N+1)$-point stencil finite difference approximation to $\partial/\partial x$ of (2.9), the original initial value problem is converted to the following system of ordinary differential equations

$$\frac{du_\ell}{dt}+\sum_{j=-N}^{N}a_j u_{\ell+j}=0, \qquad \ell=\text{integer} \tag{2.12}$$

$$t=0, \qquad u_\ell=f(\ell). \tag{2.13}$$

For the Gaussian pulse, the initial condition is,

$$t=0, \qquad u_\ell=0.5\ \exp\left[-\ell n2\left(\frac{\ell}{3}\right)^2\right]. \tag{2.14}$$

The system of ordinary differential equations (2.12) and initial condition (2.14) can be integrated in time numerically using the Runge-Kutta or a multi-step method. The solution using the standard 2^{nd}-order (N=1), 4^{th}-order (N=2), 6^{th}-order (N=3) and the optimized 7-point scheme (N=3, η=1.1) at t=400 are shown in Figure 2. The exact solution in the form of a Gaussian pulse is shown as the dotted curves. The second-order solution is in the form of a wave train. There is no resemblance to the exact solution. The numerical solution is totally dispersed. The 4^{th}-order solution is better. The 6^{th}-order scheme is even better. But there are still some dispersed waves trailing behind the main pulse. The optimized scheme gives a very acceptable numerical result.

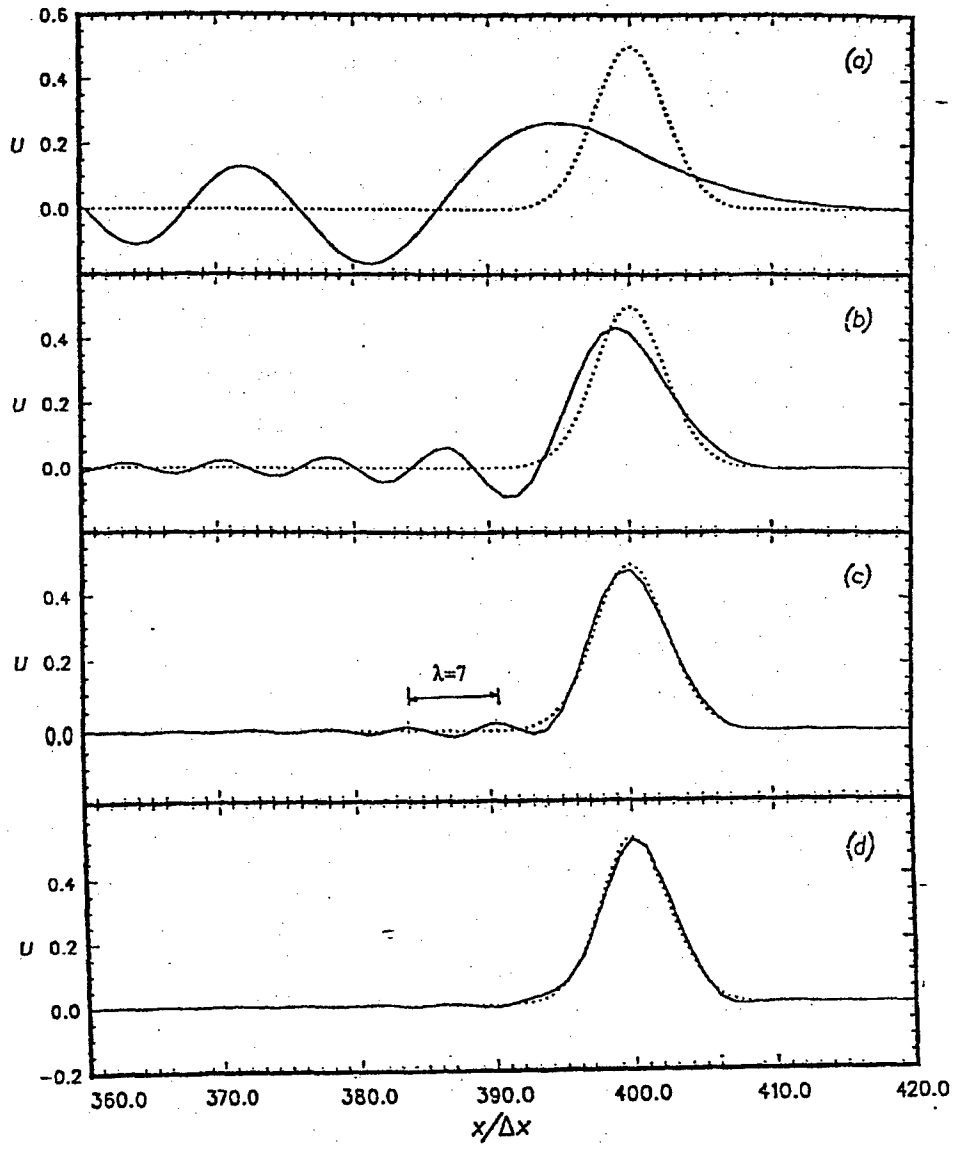

Figure 2. comparison between computed and exact solutions of the simple one-dimensional wave equation. (a) 2^{nd}-order central difference scheme. (b) 4^{th}-order central difference scheme. (c) 6^{th}-order central difference scheme. (d) DRP scheme (7-point stencil). ————numerical solution; · · · · · · · · exact solution.

3. Time Discretization

There are two types of explicit time-marching schemes. They are:

(1) Single-step scheme; e.g., Runge-Kutta method.

(2) Multi-step scheme; e.g., Adams-Bashford method.

Both types of methods are discussed in standard textbooks. Here we will only discuss the optimized multi-step method. One important advantage of multi-step method is that it can be used in a multi-size-mesh multi-time-step algorithm[2]. Such an algorithm is very efficient and nearly optimal in computation time.

Suppose **u**(t) is the unknown vector. The time axis is divided into a uniform grid with time step Δt. We will assume that the values of **u** and **du**/dt are known at time level n,n–1,n–2,n–3. (Note: In CAA, **du**/dt is given by the governing equations of motion.) To advance to the next time level, Tam and Webb[1] use the following 4-level finite difference approximation

$$\mathbf{u}^{(n+1)} = \mathbf{u}^{(n)} + \Delta t \sum_{j=0}^{3} b_j \left(\frac{\partial \mathbf{u}}{\partial t} \right)^{(n-j)} . \tag{3.1}$$

The last term on the right side of (3.1) may be regarded as a weighted average of the time derivatives at the last 4 mesh points. There are four constants, namely, b_0, b_1, b_2 and b_3. They can be determined by optimization through the use of Laplace transform. Tam and Webb suggested the following numerical values.

$$\begin{aligned} b_0 &= 2.3025580888, \quad b_1 = -2.4910075998, \\ b_2 &= 1.5743409332, \quad b_3 = -0.3858914222. \end{aligned} \tag{3.2}$$

4. Radiation and Outflow Boundary Conditions

Many interesting acoustic problems are exterior problems. To simulate this class of problems it is necessary to impose radiation and outflow boundary conditions at the boundaries of the finite computation domain. To ensure that the computed solutions are of high quality these boundary conditions must be sufficiently transparent to the outgoing disturbances so that they exit the computation domain without significant reflections. As is well known, the linearized Euler equations can support three types of waves. Thus, in general, the outgoing disturbances would contain a combination of acoustic, entropy and vorticity waves each having a distinct wave propagation characteristic. Here a set of radiation and outflow boundary conditions compatible with the optimized high-order scheme is developed starting with the asymptotic solution. A review on numerical boundary condition can be found in Ref. [4].

Consider the exterior problem involving a uniform flow of velocity u_0 in the x-direction and sound speed a_0 past some arbitrary acoustic, vorticity and entropy sources as shown in Figure 3. It will be assumed that the boundaries of the computation domain are quite far from the sources. At boundaries where there are only outgoing acoustic waves the solution is given by the following asymptotic solution,

$$\begin{bmatrix} \rho \\ u \\ v \\ p \end{bmatrix} \equiv \begin{bmatrix} \rho_a \\ u_a \\ v_a \\ p_a \end{bmatrix} = \frac{F\left(\dfrac{r}{V(\theta)} - t, \theta \right)}{r^{\frac{1}{2}}} \begin{bmatrix} \dfrac{1}{a_0^2} \\ \dfrac{\hat{u}(\theta)}{\rho_0 a_0} \\ \dfrac{\hat{v}(\theta)}{\rho_0 a_0} \\ 1 \end{bmatrix} + O\left(r^{\frac{-3}{2}} \right) \tag{4.1}$$

where $V(\theta)=a_0[M\cos\theta+(1-M^2\sin^2\theta)^{1/2}]$. The subscript '$a$' in (ρ_a,u_a,v_a,p_a) above indicates that the disturbances are associated with the acoustic waves alone. By taking the time t and r derivatives of (4.1) it is straightforward to find that for arbitrary function F of the acoustic disturbances satisfy the following equations.

$$\left(\frac{1}{V(\theta)}\frac{\partial}{\partial t}+\frac{\partial}{\partial r}+\frac{1}{2r}\right)\begin{bmatrix}\rho\\u\\v\\p\end{bmatrix}=0+O\left(r^{\frac{-5}{2}}\right). \tag{4.2}$$

Equation (4.2) provides a set of radiation boundary conditions.

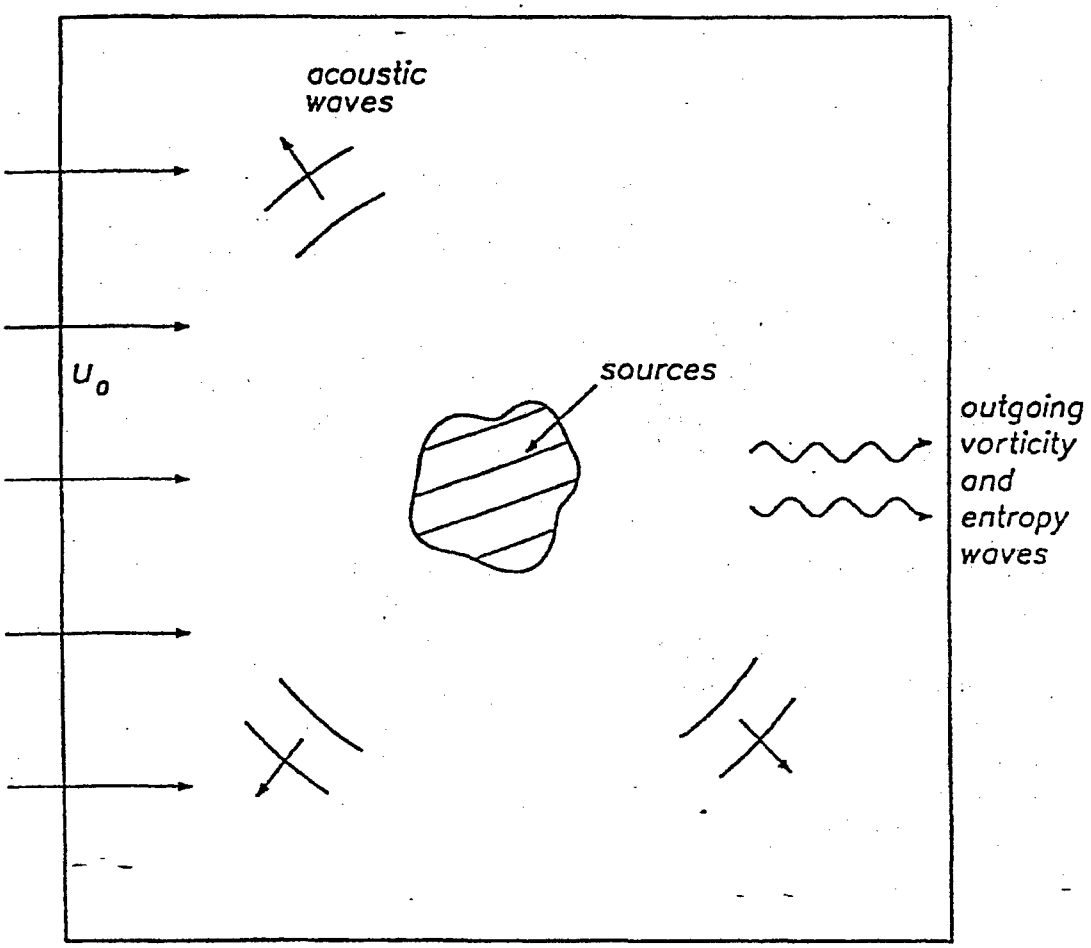

Figure 3. Acoustic, vorticity and entropy wave sources in a uniform flow.

At the outflow region, the outgoing disturbances, in general, consist of a combination of acoustic, entropy and vorticity waves. The asymptotic solutions for the density, velocity and pressure fluctuations are given by

$$\begin{bmatrix}\rho\\u\\v\\p\end{bmatrix}=\begin{bmatrix}\chi(x-u_0t,y)+\rho_a\\\dfrac{\partial\psi}{\partial y}(x-u_0t,y)+u_a\\-\dfrac{\partial\psi}{\partial x}(x-u_0t,y)+v_a\\p_a\end{bmatrix}+\ldots. \tag{4.3}$$

where the explicit form of (ρ_a, u_a, v_a, p_a) may be found in (4.1). The functions χ, ψ and F are entirely arbitrary. These functions can be eliminated by combinations of derivatives. In this way, the following outflow boundary conditions can be derived.

$$\begin{aligned}
&\frac{\partial \rho}{\partial t} + u_0 \frac{\partial \rho}{\partial x} = \frac{1}{a_0^2}\left(\frac{\partial p}{\partial t} + u_0 \frac{\partial p}{\partial x}\right) \\
&\frac{\partial u}{\partial t} + u_0 \frac{\partial u}{\partial x} = -\frac{1}{\rho_0}\frac{\partial p}{\partial x} \\
&\frac{\partial v}{\partial t} + u_0 \frac{\partial v}{\partial x} = -\frac{1}{\rho_0}\frac{\partial p}{\partial y} \\
&\frac{1}{V(\theta)}\frac{\partial p}{\partial t} + \cos\theta \frac{\partial p}{\partial x} + \sin\theta \frac{\partial p}{\partial y} + \frac{p}{2r} = 0
\end{aligned} \tag{4.4}$$

5. Artificial Selective Damping

Numerical waves of wavenumber α for which $\bar{\alpha}(\alpha)$ is not nearly equal to α (see figure 1) will not propagate with the correct wave speed. For waves on the right side of the maximum of the $\bar{\alpha}$ versus α curve of figure 1, the wave speed is negative (because $d\bar{\alpha}/d\alpha$ is negative) or opposite to the correct wave propagation direction. These are the spurious waves of the computation scheme[5]. They must be removed from the computation if a high quality numerical solution is desired. A way to do this is to apply artificial selective damping to the discretized equations. Suppose we add a damping term, $D(x)$, to the right side of the momentum equation of the linearized Euler equations in one dimension

$$\frac{\partial u}{\partial t} + \frac{1}{\rho_0}\frac{\partial p}{\partial x} = D(x). \tag{5.1}$$

Let us discretize the spatial derivative using the 7-point optimized stencil.

$$\frac{du_\ell}{dt} + \frac{1}{\rho_0 \Delta x}\sum_{j=-3}^{3} a_j p_{\ell+j} = -\frac{\nu}{(\Delta x)^2}\sum_{j=-3}^{3} d_j u_{\ell+j}. \tag{5.2}$$

In (5.2) it is assumed that D_ℓ is proportional to the values of u_ℓ within the stencil and d_j be the weight coefficients and ν is the artificial kinematic viscosity. $\nu/(\Delta x)^2$ has the dimension of $(\text{time})^{-1}$, so that d_j's are pure numbers. Now we wish to choose d_j's so that the artificial damping would be concentrated mainly on the high wavenumber or short waves.

The Fourier transform of the generalized continuous form of (5.2) is,

$$\frac{d\tilde{u}}{dt} + \_\_ = -\frac{\nu}{(\Delta x)^2}\tilde{D}(\alpha\Delta x)\tilde{u}. \tag{5.3}$$

where

$$\tilde{D}(\alpha\Delta x) = \sum_{j=-3}^{3} d_j e^{ij\alpha\Delta x}. \tag{5.4}$$

On ignoring the terms not shown in (5.3), the solution is

$$\tilde{u} \sim e^{-\frac{\nu}{(\Delta x)^2}\tilde{D}(\alpha\Delta x)t}. \tag{5.5}$$

Since $\tilde{D}(\alpha\Delta x)$ depends on the wavenumber, the damping will vary with wavenumber. For our need, we like $\tilde{D}$ to be zero or small for small $\alpha\Delta x$ but large for large $\alpha\Delta x$. This can be done by choosing d_j

appropriately. Tam, Webb and Dong[5] suggested that $\tilde{D}$ should be a positive even function of $\alpha\Delta x$. They used a Gaussian function as a template to determine d_j's. Their analysis gives the following values.

$$d_0 = 0.3276986608$$

$$d_1 = d_{-1} = -0.235718815$$

$$d_2 = d_{-2} = 0.0861506696$$

$$d_3 = d_{-3} = -0.0142811847$$

A plot of $\tilde{D}$ versus $\alpha\Delta x$ for this choice is shown in Figure 4. Figure 4 indicates that the grid-to-grid oscillations with $\alpha\Delta x=\pi$ or wavelength equal to 2 mesh spacings is most heavily damped. On the other hand, $\alpha\Delta x=0$ and the low wavenumber waves are hardly damped at all. Experience has shown that the adoption of artificial selective damping in a computation scheme can effectively eliminate all spurious short waves in the numerical solution.

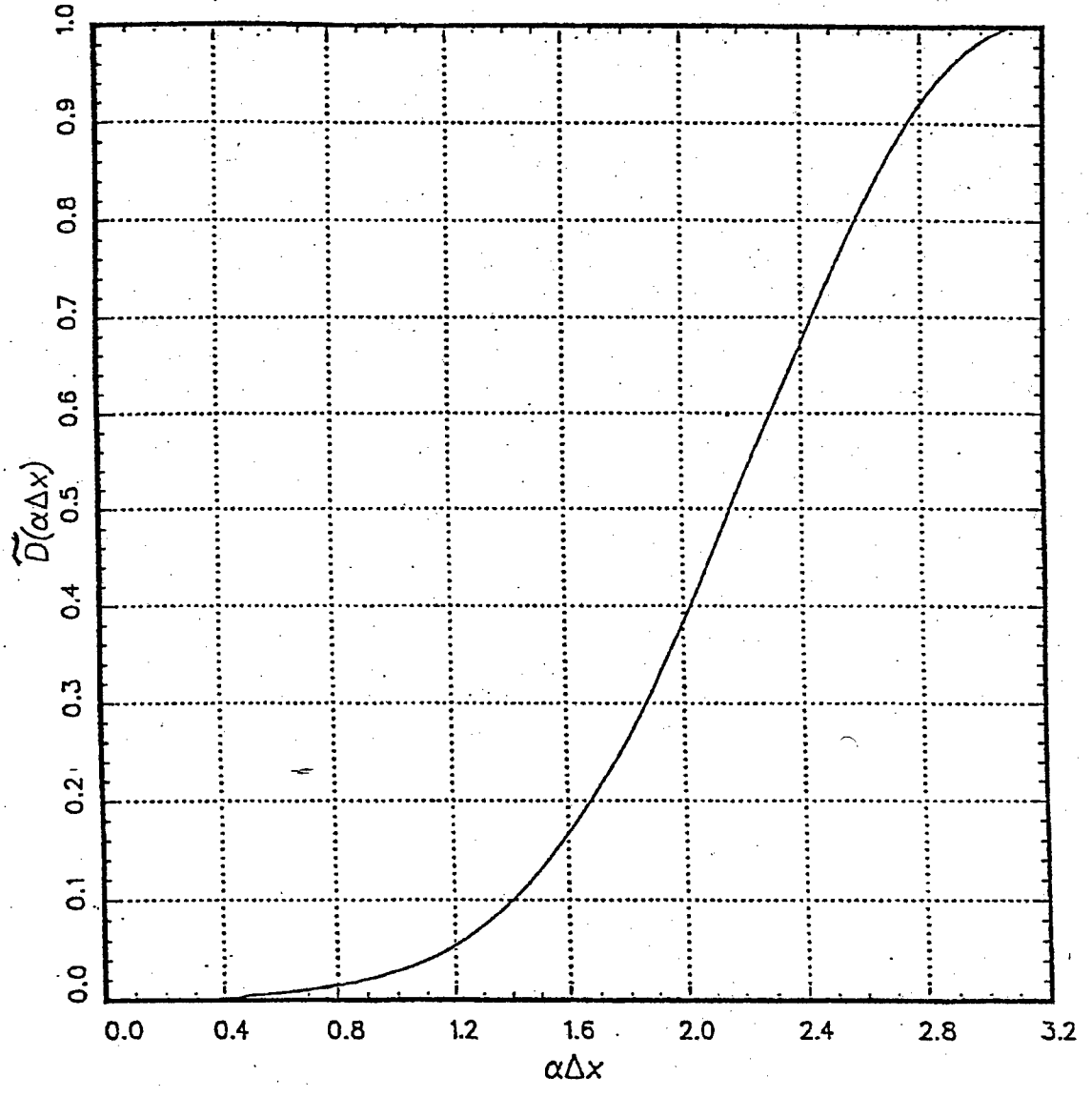

Figure 4. $\tilde{D}(\alpha\Delta x)$ versus $\alpha\Delta x$ (damping curve). $\sigma = 0.3\pi$, 7-point stencil.

6. Numerical Simulation of the Jet Screech Phenomenon

It had been reported[6–9] that structural fatigue damages sustained by the B1-A, B2-B and the F15 aircrafts were most likely the result of dynamic loading contributed by screech tones. The screech phenomenon is known to occur when a supersonic jet is imperfectly expanded. It is driven by a feedback loop. The tones are discrete frequency sound. They are generated by the interaction of downstream propagating instability waves of the jet flow and the shock cells inside the jet plume.

Experimentally, screech tones from choked jets are found to belong to four distinct modes. The A_1 and A_2 modes are axisymmetric modes with slightly different frequencies. The B and C modes are flapping modes. Their frequencies also differ only slightly. In the literature, there are semi-empirical formulas designed to predict the screech frequencies. However, these formulas are unable to predict individually the frequencies of the A_1 and A_2 modes nor the frequencies of the B and C modes. They give only a single approximate frequency for the axisymmetric modes and a single frequency for the flapping modes. The feedback loop of the screech tones is highly nonlinear. As a result, there is no tone intensity prediction formula available at the present time; not even a totally empirical one.

To provide numerical prediction of the screech frequencies and intensities as well as to better understand the physics of the problem, Shen and Tam[10–12] performed numerical simulations of the screech phenomenon. For marching the solution in time, they used the multi-size-mesh multi-time-step Dispersion-Relation-Preserving scheme. This is an improved and extended version of the optimized scheme discussed in Sections 2 and 3. Artificial selective damping was included both for the elimination of spurious short waves as well as for shock capturing purpose. In their work, a nonlinearized form of the outflow boundary conditions was used. Flow entrainment was also included in their radiation boundary condition. To simulate the effect of fine scale turbulence, the k–ε turbulence model was employed. Screech is driven by a self-excited feedback loop. Hence no external excitation is needed. In the computer simulation of Shen and Tam, the computation started from zero initial condition. In other words, the jet was turned on at time zero. After the transient disturbances had exited the computation domain, the computation locked itself onto a screech mode (sometime on two coexisting modes) automatically, exactly as in a physical experiment.

Shen and Tam[10–12] reported that their numerical simulation not only reproduced the screech frequencies of the four modes correctly but also the tone intensities were accurately given by the computed solution. Experimentally, it is observed that as the Mach number of the jet increases, at certain jet Mach numbers, there is an abrupt switch of the screech mode. This is referred to as the staging phenomenon. In the numerical simulations of Shen and Tam, the staging phenomenon was reproduced. In addition, they studied the effect of jet temperature and nozzle lip thickness on tone frequencies and intensities. Their computed results matched well with those measured experimentally[13]. Figures 5 and 6 show comparisons between the screech tone wavelengths and intensities measured from the numerical simulations of Shen and Tam[12] and the physical experiments of Ponton and Seiner[13]. As can be seen, the CAA simulations are in excellent agreement with experimental measurements over the entire range of Mach number investigated.

7. Conclusion

In this paper, computational challenges for the solution of aeroacoustics problems are discussed. To meet these challenges, specially designed high-order CAA computation schemes are developed. In addition to time marching schemes, impressive advances have also been made on numerical boundary treatment as well as on how to eliminate spurious numerical waves. As an example to illustrate the usefulness and effectiveness of these newly developed CAA methods, results of the numerical simulation of screech tones from under-expanded supersonic jets are briefly discussed. It appears that CAA has now emerged from just a novel computation method to become a powerful practical tool. CAA will undoubtedly have an enormous impact on the solution and investigation of practical aeroacoustics problems in the years to come.

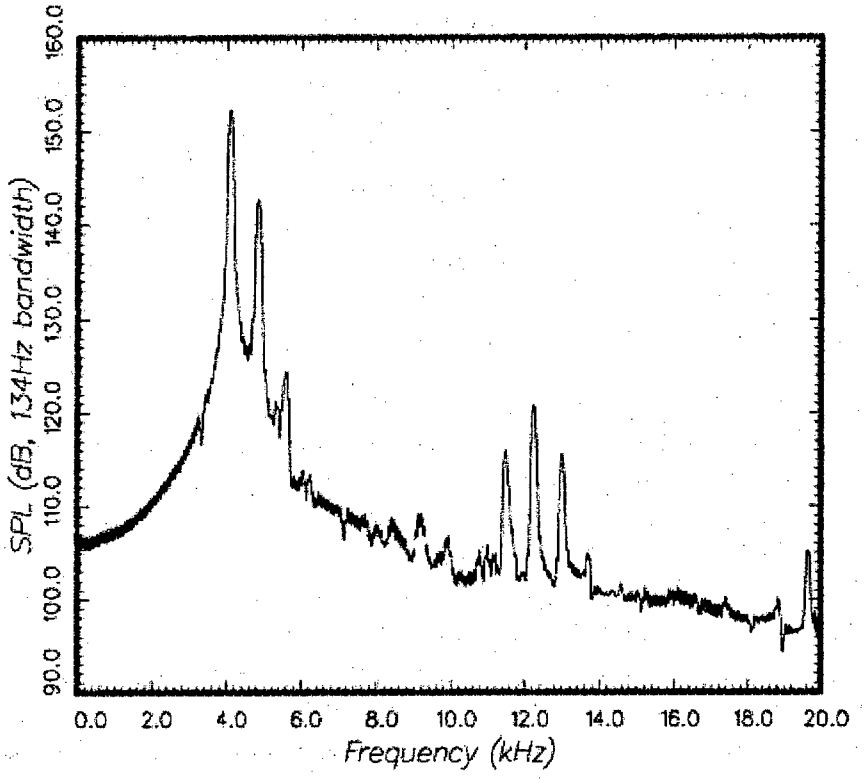

Figure 5.

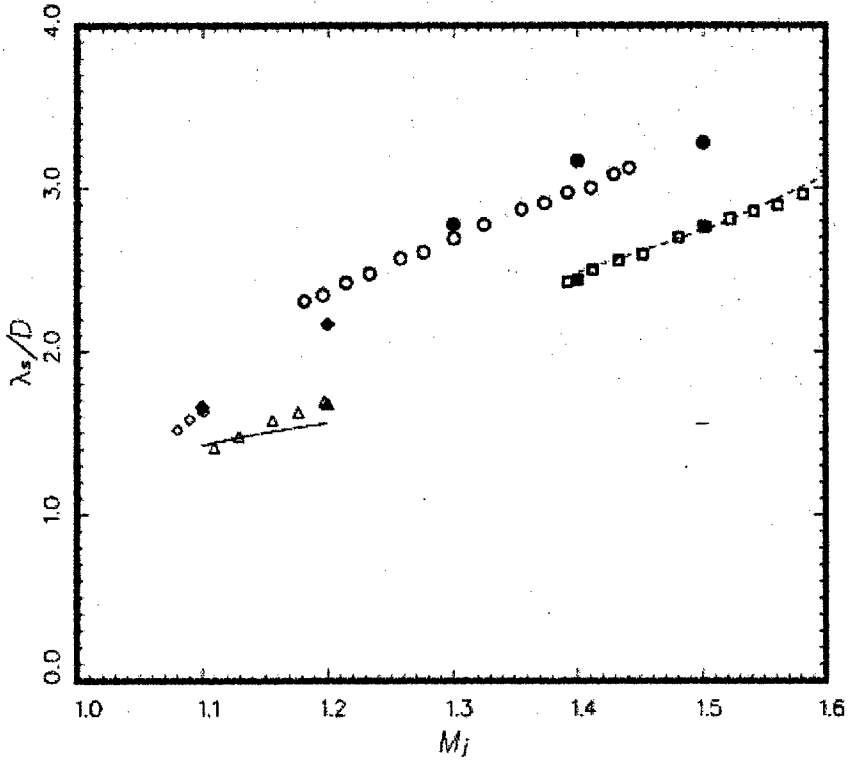

Figure 6.

Acknowledgments

This work was supported by NASA Grants NAG 3-2327, NAG 3-2102, NAG 1-2145 and NCC1-01-026

References

1. Tam, C.K.W. and Webb, J.C. Dispersion-Relation-Preserving finite difference schemes for computational acoustics. *Journal of Computational Physics*, **107**, 262–281, 1993.
2. Tam, C.K.W. Computational Aeroacoustics: Issues and Methods. *AIAA Journal*, **33**, 1788–1796, 1995.
3. Tam, C.K.W. and Kurbatskii, K.A. Multi-size-mesh multi-time-step Dispersion-Relation-Preserving scheme for multiple scales aeroacoustics problems, to appear in the *International Journal of Computational Fluid Dynamics*, 2002.
4. Tam, C.K.W. Advances in numerical boundary conditions for computational aeroacoustics. *Journal of Computational Acoustics*, **6**, 377–402, 1998.
5. Tam, C.K.W., Webb, J.C. and Dong, Z. A study of the short wave components in computational acoustics. *Journal Computational Acoustics*, **1**, 1–30, 1993.
6. Seiner, J.M., Manning, J.C. and Ponton, M.K. Dynamic pressure loads associated with twin supersonic plume resonance. AIAA Paper 85-0533, 1985.
7. Seiner, J.M., Manning, J.C. and Ponton, M.K. Model and full scale study of twin supersonic plume resonance. AIAA Paper 87-0244, 1987.
8. Shaw, L.L., Otto, C.J., Banaszak, D.L. and Plzak, G.A. F-15 8.33% model internozzle dynamic pressure environment. AFWAL-TM-86-198-FIBG, May 1986.
9. Berndt, D.E. Dynamic pressure fluctuations in the internozzle region of a twin jet nacells. Society of Automotive Engineers, Warrendale, PA, SAE-841540, Oct. 1984.
10. Shen, H. and Tam, C.K.W. Numerical simulation of the generation of axisymmetric mode jet screech tones. *AIAA Journal*, **36**, 1801–1807, 1998.
11. Shen, H. and Tam, C.K.W. Effects of jet temperature and nozzle lip thickness on screech tones, *AIAA Journal*, **38**, 762–767, 2000.
12. Shen, H. and Tam, C.K.W. Three-dimensional numerical simulation of the jet screech phenomenon. AIAA Paper 2001-0820, 2001.
13. Ponton, M.K. and Seiner, J.M. The effects of nozzle exit lip thickness on plume resonance, *Journal of Sound and Vibration*, **154**, 531–549, 1992.

Reference # of Paper: Invited Lecture #1
Discusser's Name: Dr. Brian J. Tester
Author's Name: Prof. C. K. W. Tam
Question:

The numerical simulations show energy over a broad range of frequencies. Is the broadband energy meaningful and, if so, what noise generation mechanisms does it represent?

Answer:

Because the computation took a long time to carry out the simulation was not as long as I would like. The relatively short simulation time causes the half-widths of the screech tones in the computed noise spectra to be broader than they should be. For this reason, one should not take the broadband part of the spectra too seriously.

Discusser's Name: Prof. Dr. Rolf Radespiel
Author's Name: Prof. C. K. W. Tam
Question:

By using a turbulence model in the acoustic simulation one changes the nature of the unsteady problem to be solved. Haw can you be sure not to lose relevant physical information by introducing a turbulence model?

Answer:

In the numerical simulation, a k-ε turbulence model was used to simulate the effect of the fine-scale turbulence. This is justified because of scale separation. The wavelengths of the instability waves in the jet flow are much larger than the scale of the fine-scale turbulence. This length scale disparity permits one to ignore the individual eddy motions of the fine-scale turbulence. Only the collective effect of the fine-scale turbulence on the large-scale motion is considered.

Discusser's Name: Dr. Mahmood Khalid
Author's Name: Prof. C. K. W. Tam
Question:

Did you have any difficulties with computational instabilities at the interface between the Euler and Navier-Stokes domains? Did you apply the selective artificial damping technique uniformly across the entire computational field?

Answer:

No, I have never encountered computational instabilities at the interface between Euler and Navier-Stokes regions. In the numerical simulation of jet screech, background artificial selective damping was incorporated in the computation in each computational subdomain.